Dissecting the structure-stability relationship of Y-series electron acceptors for real-world solar cell applications

Joule

CellPress

Article

Dissecting the structure-stability relationship of Y-series electron acceptors for real-world solar cell applications

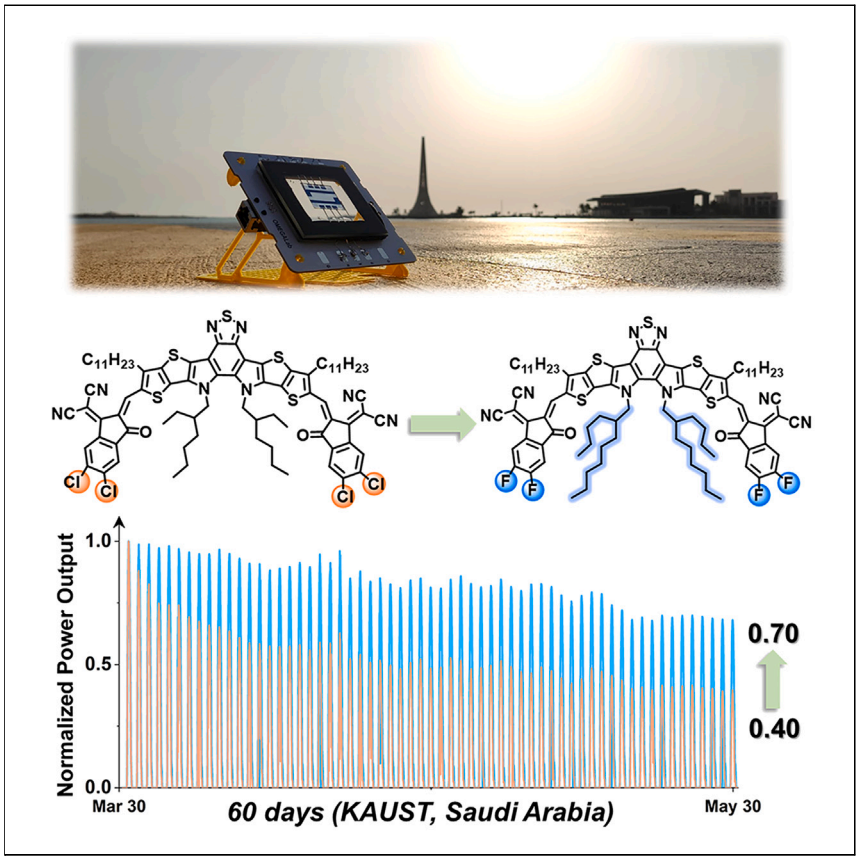

We present the outdoor performance of six Y-NFA-based organic solar cells in the hot and sunny climate of Saudi Arabia for a period of 60 days. By employing specifically designed platforms for photostability and outdoor-stability measurements, we provide chemical design guidelines of Y-NFAs for achieving outdoor stable organic solar cells, which can promote the scale-up of Y-NFA-based organic solar cells for outdoor applications.

Han Xu, Jianhua Han, Si Chen, ..., Stefaan De Wolf, Frédéric Laquai, Derya Baran

derya.baran@kaust.edu.sa

Highlights

Outdoor performance of six different Y-series NFA-based OSCs is demonstrated

Correlations between molecular structure and outdoor stability of Y-NFAs are revealed

Outdoor stability of Y-NFA cells in the Saudi climate links to photostability (~300 K)

F-end-groups and long internal side-chains in Y-NFAs improve outdoor stability

Xu et al., Joule 7, 2135–2151
September 20, 2023
https://doi.org/10.1016/j.joule.2023.07.003

Joule

CellPress

Article

Dissecting the structure-stability relationship of Y-series electron acceptors for real-world solar cell applications

Han Xu,[1,7] Jianhua Han,[1,2,7] Si Chen,[1] Ye Liu,[1] Luis Huerta Hernandez,[1] Jules Bertrandie,[1] Maxime Babics,[1] Shahidul Alam,[1] Diego Rosas Villalva,[1] Sri Harish Kumar Paleti,[1,6] Julien Gorenflot,[1] Christoph Herok,[3] Nicolas Ramos,[4] Joel Troughton,[1] Anirudh Sharma,[1] Todd B. Marder,[2] Bernd Engels,[3] Jaime Martin,[4,5] Stefaan De Wolf,[1] Frédéric Laquai,[1] and Derya Baran[1,8,*]

SUMMARY

Despite striking progress toward improving the photovoltaic (PV) performance of organic solar cells (OSCs) with recent Y-series non-fullerene acceptors (Y-NFAs), knowledge about their outdoor performance under real-world conditions and photodegradation mechanisms remains elusive, which is urgently needed to close the lab-to-fab gap of OSCs. Herein, for the first time, we study the structure-outdoor-stability relationship of Y-NFAs. We show that Y-NFAs with long internal side-chains exhibit high energy barriers for photoisomerization, and fluorinated end-groups can enhance the structural confinement to inhibit the photodegradation pathway and thereby improve device stability. Furthermore, the performance loss of Y-NFA-based OSCs under illumination is mainly driven by increased trap-assisted recombination over time. The structure-stability correlation and demonstration of outdoor performance of these state-of-the-art Y-NFA cells provided in this study highlight molecular engineering of device stability control to minimize power output losses in real-world climates.

INTRODUCTION

Organic solar cells (OSCs) have attracted extensive attention because of their light weight, mechanical flexibility, semitransparency, environmentally friendly processing, and large-area manufacturing properties.[1–7] In view of these unique advantages, solution-processed OSCs represent a transformative solar technology with excellent potential for various applications, such as powering internet of things (IoT) devices, integration into buildings, facades, and net-zero greenhouses for agriculture.[8–12] In the past few years, efforts have been devoted to designing non-fullerene acceptors (NFAs) with an A-D-A configuration (where A is acceptor and D is donor) to boost power conversion efficiencies (PCEs),[13–16] and the discovery of Y-series NFAs (Y-NFAs) began a new era for high-efficiency OSCs.[17–19] Although PCEs of the state-of-the-art OSCs have reached levels of 19% via rational molecular design of Y-NFAs,[20–22] a fundamental understanding of the relationship between the molecular structure and stability of Y-NFAs remains elusive for applications. Furthermore, the performance of these state-of-the-art Y-NFAs cells under real-world operating conditions is still unclear, and insight is urgently needed to understand the commercial potential of OSC technology.

CONTEXT & SCALE

The emergence of Y-series non-fullerene acceptors (Y-NFAs) has attracted huge attention. Y-NFA-based organic solar cells (OSCs) show excellent potential for various outdoor applications, such as building integrated photovoltaic (PV) windows and net-zero greenhouses. However, their performance in real-world climates has not been documented so far. Herein, we report outdoor performance of Y-series solar cells and reveal correlations between molecular structure and outdoor stability of Y-NFAs for the first time. We elucidate how outdoor stability of Y-NFA cells in hot Saudi climates is strongly connected to their photostability at 300 K. Fluorinated end-groups and long internal side-chains in Y-NFAs can suppress the photodegradation pathway and thereby enhance outdoor stability. A photostable Y-NFA system that prevents light-induced degradation would be required to achieve commercial viability for outdoor applications.

Device lifetime under real-world operating conditions of photovoltaic (PV) technologies is mainly affected by ambient moisture and oxygen ingress, light, and heat.[23–26] Diffusion of oxygen and moisture into PV devices in real-world climates can be suppressed through successful encapsulation processes.[27] For heat-induced degradation of Y-NFA-based solar cells, a molecular architecture with a high glass transition temperature that prevents the diffusion of Y-NFAs is required to achieve thermally stable OSCs.[28–31] For light-induced degradation of NFAs, *cis-trans* isomerization of vinyl groups under illumination is an important degradation pathway for the A-D-A type NFAs, followed by epoxide formation or electrocyclization with an isomeric photodegradation product.[32–35] Such a conformational change is attributed to the photodegradation process and observed across the families of A-D-A type NFAs including IDTBR, IDFBR, ITIC, and IEICO-series NFAs (detailed chemical structures in Figure S1).[32,34–36] Generally, Y-NFAs are more photostable than ITIC-series NFAs, and the *cis-trans* isomerization of vinyl groups in Y-NFAs could be suppressed to a certain extent because of the steric effect induced by outer side-chains (Figure 1A).[32,34,35] Nonetheless, Y-NFAs still exhibit non-negligible degradation behaviors and suffer from device performance loss under illumination. Recently, Wang and coworkers investigated the correlation between the side-chains of NFAs and their chemical, morphological, and photostability using ZnO as the electron extraction layer.[37] Jen et al. found that the large structural hinderance induced by the outer side-chains in Y-NFAs improves thermal stability of the devices, and the Y-NFA with brominated thiophene side-chains (large side-group torsion) yielded decent photostability in devices.[38] However, the intrinsic correlation between structure-photostability of Y-NFAs excluding ZnO-induced photocatalytic degradation, remains elusive. Thus, in-depth investigation of light-induced degradation of Y-NFAs is of great importance for understanding structure-stability relationships of the state-of-the-art OSCs.

Performance loss of OSCs in real-world climates would provide device stability data and guide the research community,[39,40] which can narrow the lab-to-fab gap. To gather reliable outdoor stability results, an outdoor lifetime testing platform needs to be constructed that is able to measure devices following the International Summit on Organic Photovoltaic Stability (ISOS) protocols.[40] In the past few years, only limited studies on the outdoor performance of NFA-based OSCs have been reported. Greenbank et al. compared the outdoor degradation behavior of ITIC- and fullerene-based devices, and Josey et al. investigated the outdoor performance of devices based on boron subphthalocyanine acceptors.[41,42] However, the device efficiencies in these reported studies are less than 8%, which is not representative of state-of-the-art OSCs and lags far behind the development of Y-NFAs. Recently, Inganäs and coworkers reported the outdoor stability of the laminated organic PV modules using all-polymer blends (PYF-T-o as acceptor, polymerized Y-NFA with thiophene units).[43] Thus far, the correlation between molecular structures of Y-NFAs and their outdoor stability is still unclear, reflecting the limited understanding of how a photostable Y-NFA shapes the resulting outdoor performance and how molecular structures govern the outdoor stability of Y-NFA cells. Therefore, exploration of structure-stability relationships and outdoor performance of these state-of-the-art Y-NFAs will further promote the scaling up of OSCs.

In this work, we establish design guidelines for Y-NFAs by studying the structure-stability behavior of Y-NFAs with poly[(2,6-(4,8-bis(5-(2-ethylhexyl-3-fluoro)thiophen-2-yl)-benzo[1,2b:4,5-b′]dithiophene))-alt-(5,5-(1′,3′-di-2-thienyl-5′,7′-bis(2-ethylhexyl) benzo[1′,2′-c:4′,5′c′]dithiophene-4,8-dione)] (PM6) as the donor (for the materials and chemical structures, see Figure S1). First, we investigated the photostability

[1]King Abdullah University of Science and Technology (KAUST), Physical Sciences and Engineering Division (PSE), KAUST Solar Center (KSC), Thuwal 23955-6900, Kingdom of Saudi Arabia

[2]Institut für Anorganische Chemie and Institute for Sustainable Chemistry & Catalysis with Boron (ICB), Julius-Maximilians-Universität Würzburg, Am Hubland, 97074 Würzburg, Germany

[3]Institut für Physikalische und Theoretische Chemie, Julius-Maximilians-Universität Würzburg, Am Hubland, 97074 Würzburg, Germany

[4]POLYMAT, University of the Basque Country UPV/EHU, Av. De Tolosa 72, 20018 San Sebastián, Spain

[5]Ikerbasque, Basque Foundation for Science, Bilbao 481013, Spain

[6]Department of Chemistry and Chemical Engineering, Chalmers University of Technology, 41296 Göteborg, Sweden

[7]These authors contributed equally

[8]Lead contact

*Correspondence: derya.baran@kaust.edu.sa

https://doi.org/10.1016/j.joule.2023.07.003

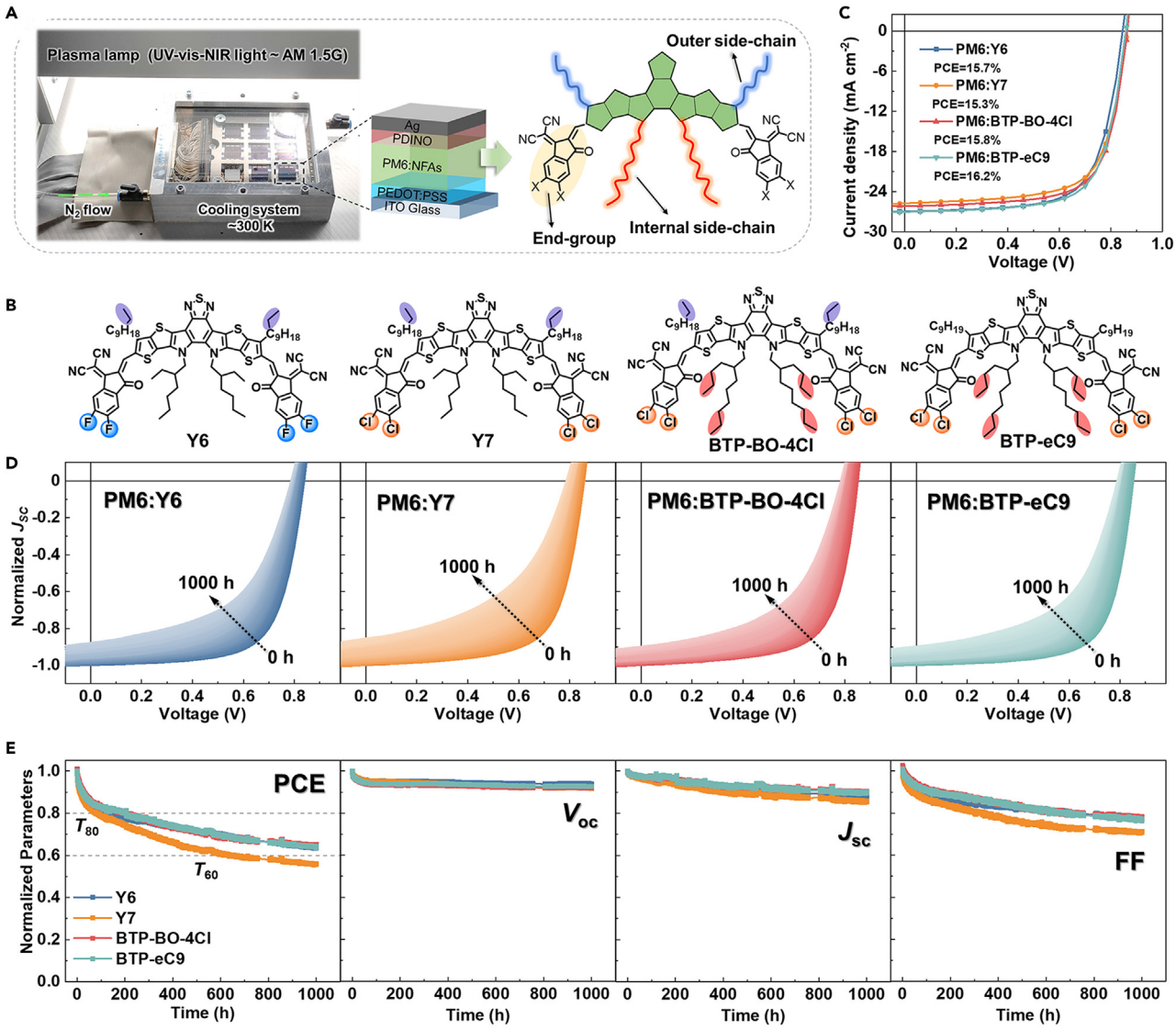

Figure 1. Photovoltaic performance and photostability results

(A) Photostability measurement chamber and conventional device structure.

(B) Chemical structures of Y6, Y7, BTP-BO-4Cl, and BTP-eC9.

(C) *J-V* curves on champion devices based on the different acceptors. Photovoltaic parameters of these Y-NFA:PM6-based devices are given in Table S2. The *J-V* curves were obtained every 10 min.

(D) *J-V* curves during 1,000 h of continuous illumination. The J_{sc} values are normalized to the respective J_{sc} at t = 0.

(E) PV parameters during photostability tests. The PV parameters are normalized to the respective PV parameters at t = 0.

behavior of OSCs based on different Y-NFAs: Y6, Y7, BTP-BO-4Cl, and BTP-eC9.[17,44–46] These Y-NFAs enable us to compare the influence of different end-groups, internal side-chains, and outer side-chains on the photodegradation behaviors of Y-NFAs. We found that the degradation of fill factor (FF) in the *J-V* characteristics is the main manifestation of a lack of photostability at the device level, which results from the enhanced light-induced trap-assisted recombination as identified by light-intensity dependence measurements and time-delayed collection field (TDCF) characterizations. Through transition-state calculations, we show that a long internal side-chain endows Y-NFAs with high energy barriers for the rotation of end-groups and inhibits the photodegradation pathway, which agrees well with

device performance. This concept is further demonstrated by using two other Y-NFAs: N3 and Y12 bearing longer internal side-chains exhibiting better photostability than Y6.[47,48] Lastly, we evaluated and compared the outdoor performance of the Y-NFA-based OSCs following the ISOS-O-2 protocol (outdoor sunlight as light source with environmental temperature and humidity and loading at open-circuit condition).[24] With the help of our custom-designed, cost-effective, and open-source hardware-software stability platform, we are able to track lab-scale devices reliably. We demonstrate that the proposed structure-photostability relationships of Y-NFA cells (temperature ~300 K) are also relatable to their outdoor stability in hot Saudi climates. Importantly, the structure-stability correlation and demonstration of outdoor performance of Y-NFA cells provided by this study highlight that molecular engineering on outdoor stability is one of the key factors to minimize losses of output power in OSC under real-world operating conditions.

RESULTS AND DISCUSSION

A photograph of the photostability measurement for observing the light-induced degradation of solar cells under controlled lab-environment conditions is presented in Figure 1A. Conventional architecture solar cells were held in a metallic chamber under continuous light generated from a plasma lamp system in an N_2 atmosphere. In comparison with the commonly used light-emitting diodes (LEDs) and metal halide lamps, the spectrum of the plasma lamp used in this study includes UV and infrared light, which is close to the standard AM 1.5G solar irradiation (Table S1; Figure S2) and also correlates with the solar-harvesting behavior of Y-NFAs. The cooling system maintained the devices at ca. 300 K to eliminate heat-induced degradation, and continuous N_2 flow was used to prevent water and oxygen ingress. The photostability results were automatically collected by a computer in 10-min intervals and gathered following the ISOS-L-1 protocol (solar simulator as light source with controlled temperature and humidity, loading at open circuit).[24] Figure 1A shows the structural architecture of Y-NFAs: dithienothiophen[3.2-b]-pyrrolobenzothiadiazole (BTP) core with different end-groups and internal and outer alkyl side-chains. To identify the influence of structural factors, we initially selected four acceptors: Y6, Y7, BTP-BO-4Cl, and BTP-eC9 (Figure 1B). Comparison between Y6 and Y7 can reveal the difference between the fluorinated and chlorinated end-groups. Y7 has shorter internal side-chains than BTP-BO-4Cl, and BTP-BO-4Cl has longer outer side-chains than BTP-eC9 (revealing the effects of the length and location of side-chains). In the presence of oxygen, donor polymers such as PM6 act as weak links in the photostability of Y-NFA-based devices.[49,50] In the absence of oxygen (under conditions such as photostability testing according to ISOS-L-1 or devices with high-quality encapsulation), some groups have reported that Y-NFA-based devices show photodegradation behavior in both PM6 and Y6.[51–54] In this work, to investigate systematically the degradation behaviors of Y-NFAs under illumination covering both UV-vis-NIR (ultraviolet-visible-near-infrared) light, we used the same batch of PM6 as the donor and fabricated conventional devices, indium-tin-oxide (ITO, 180 nm)/poly(3,4-ethylenedioxythiophene):poly(styrenesulfonate) (PEDOT:PSS, 30 nm)/PM6:Y-NFAs (~100 nm)/perylene diimide functionalized with amino *N*-oxide (PDINO, 10 nm)/Ag (100 nm), for the photostability measurements and characterization. The photoactive layers were all treated with an identical thermal annealing process (100°C for 10 min), and no additives were involved to prevent any further potential influence on photostability. The selection of PDINO is based on our photostability results and is shown to be the most stable candidate among the studied electron transport layers in Figure S3. As shown in Figures 1C and S4 and Table S2, the devices based on these acceptors all exhibit similarly high PCEs

ranging from 15.3% to 16.2%, which are representative for analyzing their photostability behaviors.

Figure 1D depicts the changes in *J-V* curves during 1,000 h of illumination for the four Y-NFA-based devices (the averaged PCE changes based on five devices of each type; Figure S5). Normalized PCE, open-circuit voltage (V_{OC}), short-circuit current (J_{SC}), and FF are shown in Figure 1E. Device lifetimes (T_{80}, representing the time a device can retain >80% of its initial PCE) of the Y6-, Y7-, BTP-BO-4Cl-, and BTP-eC9-based devices are 107, 79, 205, and 205 h, respectively. After the initial burn-in period, the drop of V_{OC} becomes much slower. However, alongside J_{SC} dropping mildly, the FF dropping is still fast and becomes the main reason for the PCE loss. In comparison with the devices with Y6, BTP-BO-4Cl, and BTP-eC9, the device fabricated from Y7 with chlorinated end-groups and short internal side-chains exhibits the highest rate of PCE loss, retaining only 56% of its initial PCE after 1,000 h of illumination. T_{60} for the Y7-based devices is 664 h, which is much shorter than the ones from the other three Y-NFA devices (T_{60} > 1,000 h). The devices fabricated with BTP-BO-4Cl and BTP-eC9 have similar photodegradation behaviors, indicating that the length of the outer side-chain (from $-C_{11}H_{23}$ to $-C_9H_{19}$) has a negligible effect on the photostability of Y-NFAs. It is worth mentioning that Jen et al. recently showed that local-isomerized conjugated outer side groups with large steric effect can balance the efficiency and photostability of the OSCs.[55] For the alkyl side-chains in this study, the Y-NFA with fluorinated end-groups and longer internal side-chains exhibits better photostability than its counterparts.

We further utilized fresh and aged devices after 300 h of illumination to investigate the photodegradation mechanism. Photocurrent density (J_{ph}) vs. effective voltage (V_{eff}) measurements were involved in comparing the exciton dissociation probability. The exciton dissociation efficiency, *P*(E,T) is extracted from the J_{ph}-V_{eff} curves (Figure S6) and summarized in Figure 2A. All of the fresh devices exhibit high *P*(E,T) values: 95.5% for Y6, 95.0% for Y7, 97.3% for BTP-BO-4Cl, and 96.1% for BTP-eC9-based devices, which agree well with their high PCEs. After illumination, the Y7-based device, as the most unstable device, exhibits the lowest *P*(E,T) value (88.1%) among all the four Y-NFA devices. To gain additional insight into the charge transport behavior before and after illumination, photo-induced charge carrier extraction by linearly increasing voltage (photo-CELIV) measurements were employed (Figures 2B and S7).[56] Similar to the *P*(E,T) results, all four devices exhibit decreased charge carrier mobilities after illumination. The changes of J_{SC} with respect to light intensity are plotted on logarithmic scales (Figure S8), and the slopes (α) of the fitting lines are summarized in Figure 2C. For all of the Y-NFA-based devices, α values are basically unchanged before and after photoaging (around 0.96 and close to 1), indicating that bimolecular recombination is not the main reason for the performance degradation. However, the values of the ideality factor (*n*) calculated from V_{OC} vs. light-intensity curves (Figure S9) show significant differences between the fresh and aged devices. As presented in Figure 2D, the *n* values of fresh devices based on Y6, Y7, BTP-BO-4Cl, and BTP-eC9 are all close to 1. After 300-h illumination, the *n* values of all aged devices are significantly increased, indicating trap-assisted recombination.

To elucidate further differences in geminate recombination and bimolecular recombination prior to and after photoaging, we performed TDCF measurements varying the pre-bias during photoexcitation (Figure S10).[57] The normalized total extracted charge at different pre-bias voltages (V_{pre}) is plotted in Figure 2E to compare geminate recombination in fresh and aged devices. We note that even fresh devices

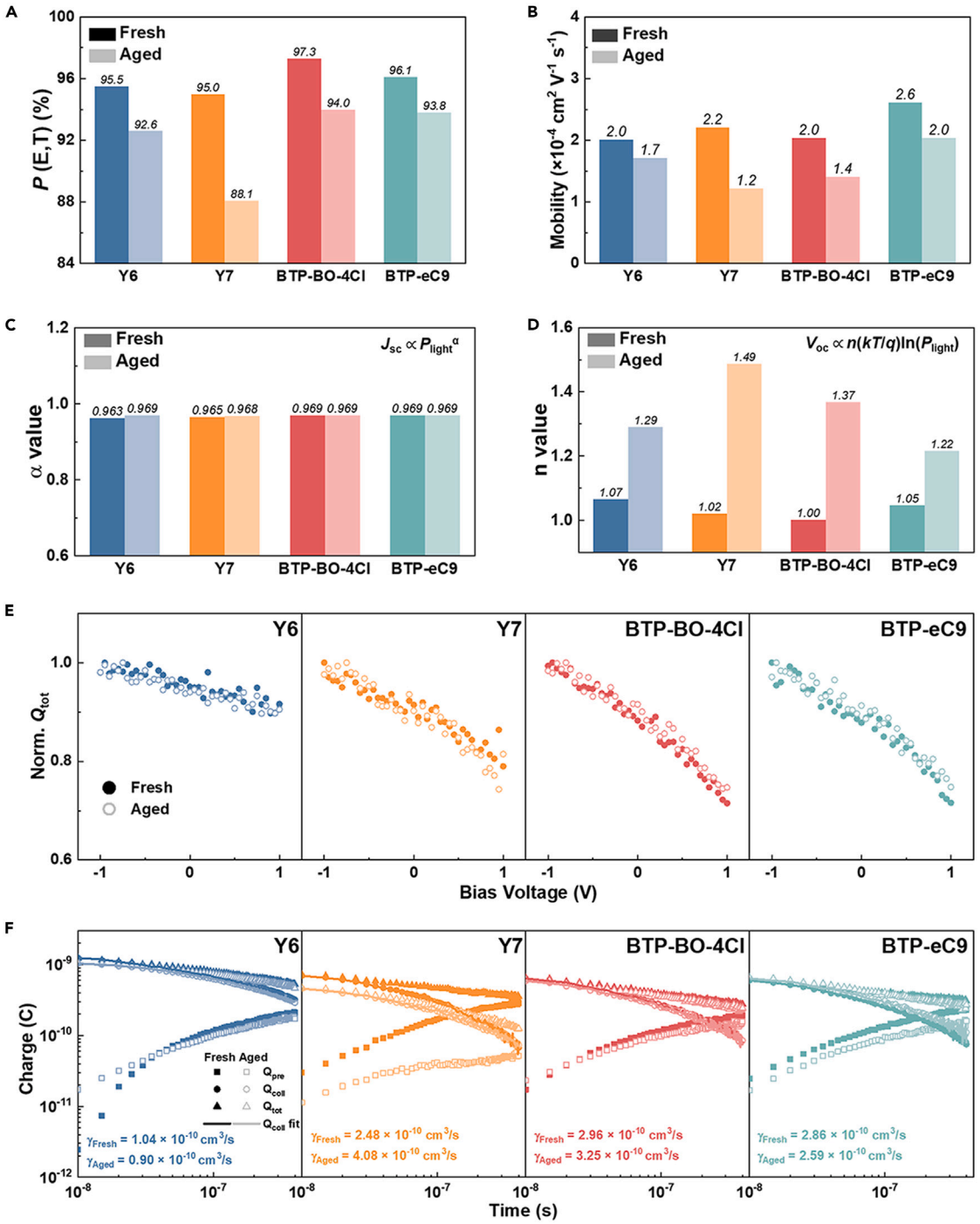

Figure 2. Physical mechanisms of the fresh and aged devices

(A) *P*(E,T) values of the fresh and aged devices.

(B) Mobilities of the fresh and aged devices extracted from photo-CELIV measurements.

(C and D) α values and *n* values before and after illumination.

(E) Total extracted charge as a function of the applied pre-bias during laser excitation at 532 nm, normalized to the maximum Q_{tot} around −1 V. The pulse fluence was 0.03 μJ/cm^2 and the time delay was 15 ns.

(F) Q_{tot}, Q_{coll}, and Q_{pre} as a function of the delay time during laser excitation at 532 nm. The pulse fluence was 0.1 μJ/cm^2. Bimolecular recombination coefficients extracted from TDCF measurements.

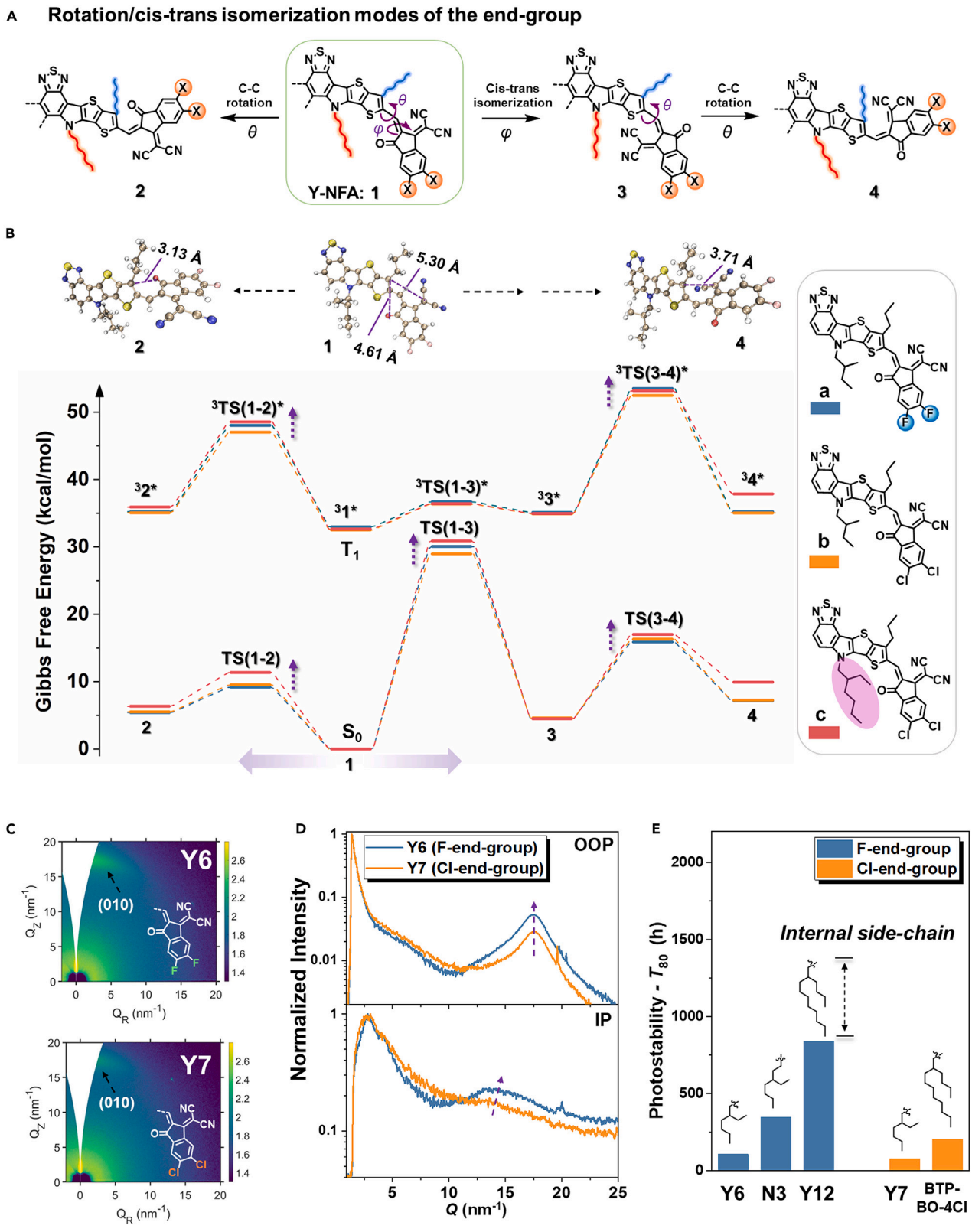
A
Rotation/cis-trans isomerization modes of the end-group
C-C rotation
θ
Cis-trans isomerization
φ
C-C rotation
θ
2
Y-NFA: 1
3
4
B
3.13 Å
5.30 Å
3.71 Å
4.61 Å
2
1
4
Gibbs Free Energy (kcal/mol)
3TS(1-2)*
3TS(1-3)*
3TS(3-4)*
32*
31*
33*
34*
T1
TS(1-3)
TS(1-2)
TS(3-4)
S0
a
b
c
C
Y6
(010)
Y7
(010)
QZ (nm-1)
QR (nm-1)
D
Y6 (F-end-group)
Y7 (Cl-end-group)
OOP
IP
Normalized Intensity
Q (nm-1)
E
F-end-group
Cl-end-group
Internal side-chain
Photostability - T80 (h)
Y6
N3
Y12
Y7
BTP-BO-4Cl

Figure 3. DFT calculations and morphological characteristics

(A) Rotation modes of the end-group in Y-NFAs.

(B) Energy profiles for the reaction pathways and the molecular geometries of component a. Activation energy values are given in Table S4, and the imaginary vibrational modes for the transition states are shown in Figure S20. Considering the long side-chains in Y-NFAs, we also performed dispersion-corrected DFT calculations (DFT-D3), and the results are summarized in Table S4. The excited singlet state pathway is shown in Figure S21 and Table S5 (discussion in Note S5).

(C and D) GIWAXS patterns and 1D cut-lines of the Y6 and Y7 neat films.

(E) Device lifetimes (T_{80}) of the PM6:Y-NFA cells. Photostability of the N3- and Y12-based devices, see Figure S25.

exhibit an electric field dependence of charge generation, which is smallest for Y6-based devices. However, for all four systems, the electric field dependence of charge generation is virtually unaffected by aging. Therefore, changes in the field dependence and fraction of geminate charge recombination cannot account for the decreased FF observed in aged devices. Thus, we further investigated non-geminate charge pair recombination via TDCF in fresh and aged devices. We obtained the bimolecular recombination coefficient, γ, by fitting the total charge collected, Q_{coll}, which had not recombined after pulsed laser excitation as a function of the delay time, t_d, prior to the application of the extraction voltage. Here, Q_{coll} is corrected for the amount of charge, Q_{pre}, that manages to escape the device prior to t_d, although kept at V_{OC}[58]:

$$Q_{coll(t_d+\Delta t)} - Q_{coll(t_d)} = -\left[Q_{pre_{(t_d+\Delta t)}} - Q_{pre_{(t_d)}}\right] - \gamma \frac{Q_{coll(t_d)}^{2}}{eAd}\Delta t,$$

where A and d represent the device area and active layer thickness, respectively. Typically, the γ values extracted from TDCF measurements are of the order $\sim 10^{-11}$ cm^3 s^{-1} for high-efficiency Y-NFAs.[57,59] As shown in Figure 2F, γ values of the fresh devices based on Y6, BTP-BO-4Cl, and BTP-eC9 range from 1.04 to 2.96 × 10^{-10} cm^3 s^{-1}, indicating increased bimolecular recombination compared with literature-reported values of high-efficiency devices. We hypothesize that this is due to the preparation protocol used here for the devices, which did not include any additives or post-processing treatments. Moreover, the γ values of the fresh and aged devices all exhibit very small changes. Taking into account the results of light-intensity-dependent J_{SC} and V_{OC} measurements and the results of the TDCF experiments, it appears that light-induced trap-assisted recombination constitutes the most significant contribution to the FF decrease. A notable exception is the following: for the Y7-based device only, a slightly larger increase of the γ value suggests that additional recombination losses may worsen the FF degradation. In fact, the performance of PM6:Y-NFA-based devices is comparably stable at room temperature (shelf life stability in Figure S11, only 5% to ~10% performance loss after 300 h)[60–62] Therefore, the increased recombination and PCE losses observed in the photostability measurements (Figure 1E) appear to be primarily related to the possible chemical structural change caused by continuous illumination.

As shown in Figure 3A, it has been reported that the vinyl groups in NFAs undergo photoisomerization followed by electrocyclic reaction under illumination.[32,34,35] Theoretically, the existence of outer side-chains in Y-NFAs could limit the photoisomerization process in comparison with ITIC, IEICO, and IDTBR-series NFAs (Figure S1).[32,33,35] Herein, we observe that Y-NFAs still exhibit photodegradation under illumination. Figure S12 shows Raman spectra of the Y6 neat films before and after photoaging. There is a quenching of the peaks from 1,100 to 1,450 cm^{-1} and slightly increased peaks at ~1,590 and ~1,690 cm^{-1} after 100 h of illumination as observed experimentally. These changes agree well with the density functional theory (DFT)-simulated Raman spectra and reported studies,[33,35] confirming that the twisting and

loss of conjugation between core and end-group could be the reason for the photodegradation (Figures S13–S15). Such structural changes and photodegradation behaviors are also observed from the ^{1}H-NMR (nuclear magnetic resonance) spectra (Figure S16). However, for the neat Y-NFA films, it is difficult to quantify the photodegradation rate by NMR techniques due to variations in thickness and aggregation properties of different Y-NFAs, as shown in Figure S16A. Generally, there are two different rotation modes of the vinyl group in A-D-A-type NFAs, as presented in Figure 3A. The first one is a *cis-trans* isomerization (1 → 3 → 4) that leads to the formation of a cyclic byproduct between the dicyanomethylene unit and the thiophene ring, which was identified by Perepichka et al.[32] The second one is an alternative but similar isomerization (1 → 2) that leads to the formation of a pyran ring, which is considered to be another product (not a primary degradation product) by Kim et al. (as summarized in Figure S15).[35] We then simulated NMR spectra for the possible photodegradation products of Y6 (Figure S17). The results of Raman and NMR spectra show that the photodegradation pathway most frequently follows the isomerization direction of 1 → 3 → 4, which agrees well with the reported work (Note S1).[35] We also measured the UV-vis absorption of these Y-NFAs before and after photoaging under a plasma lamp (including both UV and NIR light). As shown in Figure S18, these Y-NFAs exhibit decreased UV-vis absorption behaviors after illumination due to the breakage of conjugation with vinyl groups (Note S2). To confirm the link between the chemical degradation pathway of Y-NFAs and the performance loss of the devices, we simulated the UV-vis absorption spectra (Figure S19) and photophysical properties of the possible degradation products of Y6.[63–67] As shown in Table S3, the degradation products result in increased energetic disorders, which can lead to increased trap-mediated recombination. Additionally, the increased singlet-triplet energy gaps caused by the degradation products could result in more triplet-mediated recombination. Both of these effects induced by the photodegradation products can contribute to a decline in device performance (Note S3).[32,63,65,67]

To understand the end-group and side-chain effects on photostability of Y-NFAs at the molecular level, DFT-predicted activation energies along with the reaction path (at the CAM-B3LYP/6-31G(d,p) level of theory) were performed. Herein, as shown in Figure 3B and Table S4, we calculated the transition states following both of the two photoisomerization pathways. The structures of Y-NFAs for transition-state calculations are truncated after the benzothiadiazole core to minimize the computational cost (discussion in Note S4). Generally, the triplet states (T_1) in organic semiconductors have longer intrinsic lifetimes than the first excited singlet states (S_1).[68,69] It is also known that the formation of T_1 through the back charge transfer pathway in PM6:Y6 blends is responsible for the dominant (non-geminate) charge recombination and even device degradation.[63] Therefore, compared with the S_1 pathway, the T_1 pathway is likely to be more relevant for photoisomerization degradation (see Note S5 for a detailed discussion of the S_1 and T_1 pathways). Herein, higher activation barriers are predicted for the Y-NFAs with long internal side-chains (compound **c**) compared with the ones with short internal side-chains (compounds **a** and **b**) for the TS(1–2), TS(1–3), and TS(3–4) along the ground state (S_0) and T_1 pathways. This indicates that the internal side-chain can effectively hinder the rotation of the end-groups in Y-NFAs because of the steric effect. Considering the long, soft side-chains in Y-NFAs, we also performed transition-state calculations incorporating the empirical atom-atom dispersion corrections (DFT-D3).[70] As shown in Table S4, in comparison with the short internal side-chains, the long internal side-chains still yield high energy barriers along with the reaction paths. The results from transition-state calculations show that the activation energy for photoisomerization required for the

derivative with fluorinated end-groups (compound **a**) is quite similar to the one with chlorinated end-groups (compound **b**).

Grazing incidence wide-angle X-ray scattering (GIWAXS) measurements were performed to check the structural confinement effect in condensed films (Figure S22; Table S6; Note S6). As shown in Figures 3C and 3D, although these Y-NFAs have similar π-π stacking distances in the out-of-plane (OOP) direction, Y6 with fluorinated end-groups exhibit stronger π-π stacking intensities both in OOP and in-plane (IP) directions and also smaller d-spacing in the IP direction in the condensed films than their counterparts with chlorinated end-groups (GIWAXS results for the Y7 and BTP-BO-4Cl films; Figure S23). Such dense molecular packing can provide structural confinement in the condensed solid and suppress the photoisomerization of Y-NFAs under illumination. In addition, fluorine is the most electronegative element in the periodic table; its Pauling electronegativity is 4.0, which is higher than that of chlorine (3.2).[71] It is known that fluorinated aromatic units can induce strong π-stacking interactions in conjugated molecular systems, which was first reported by Patrick and Prosser.[72,73] We further calculated the electrostatic maps of the fluorinated and chlorinated Y-NFAs. As shown in Figure S24, compared with the chlorinated Y-NFA, the fluorinated Y-NFA shows more positively charged phenyl and negatively charged halogen atoms in the end-groups, which is induced by the strong electron-withdrawing effect of the fluorine. Recently, Kim et al. also reported that the calculated quadrupole moment of Y6 (191.7 ea_0^2) is higher than the one of Y7 (175.7 ea_0^2), and such fluorine-induced strong coupling and quadrupole-quadrupole interactions in BHJ blends could prevent the photodegradation of end-groups and enhance the photostability of NFAs.[35] We also summarized the quadrupole moments of another 16 different NFAs with fluorinated and chlorinated end-groups from the previous work.[74] As shown in Figure S24, the quadrupole moments of NFAs with F-end-groups are both higher than those with Cl-end-groups. Such large quadrupole moments enable strong intermolecular interactions, leading to the strong confinement of end-groups and suppressing the photodegradation pathway.

Following the above structural guidance, we fabricated devices based on the Y-NFAs with F-end-groups and longer internal side-chains: N3 and Y12 (the molecular structures in Figure S1) to examine the structure-stability relationship. The N3- and Y12-based devices also exhibit similarly high PCEs of 15.4% and 15.5% (Table S1), respectively, which are representative for comparing their photostability behaviors (see the *J-V* curves in Figure S4 and the photostability results in Figure S25). As shown in Figure 3E, with fluorinated end-groups, devices based on longer internal side-chain showed better stability. Compared with Y6-based devices, N3- and Y12-based devices both exhibited higher device T_{80} lifetimes of 348 and 837 h, respectively. Moreover, the Y-NFAs with fluorinated end-groups (Y6 and Y12) are also more photostable than the ones with chlorinated end-groups (Y7 and BTP-BO-4Cl). The structure-stability relationship in Figure 3E agrees well with our DFT and GIWAXS analyses.

Finally, we evaluated the outdoor performance of these Y-NFA-based devices. The devices were encapsulated in thermoplastic polyurethane to prevent the diffusion of water and oxygen into the PV devices.[27] The outdoor measurements were carried out using our specially designed equipment as shown in Figure 4A, namely, a multi-channel source-measure unit based on our open-source source meter unit (μSMU, https://certification.oshwa.org/sa000002.html) calibrated against a Keithley 2400 SMU (for the fabrication and experimental details, see supplemental information and Figure S26).[75] *J-V* curves of the devices were recorded at time intervals of

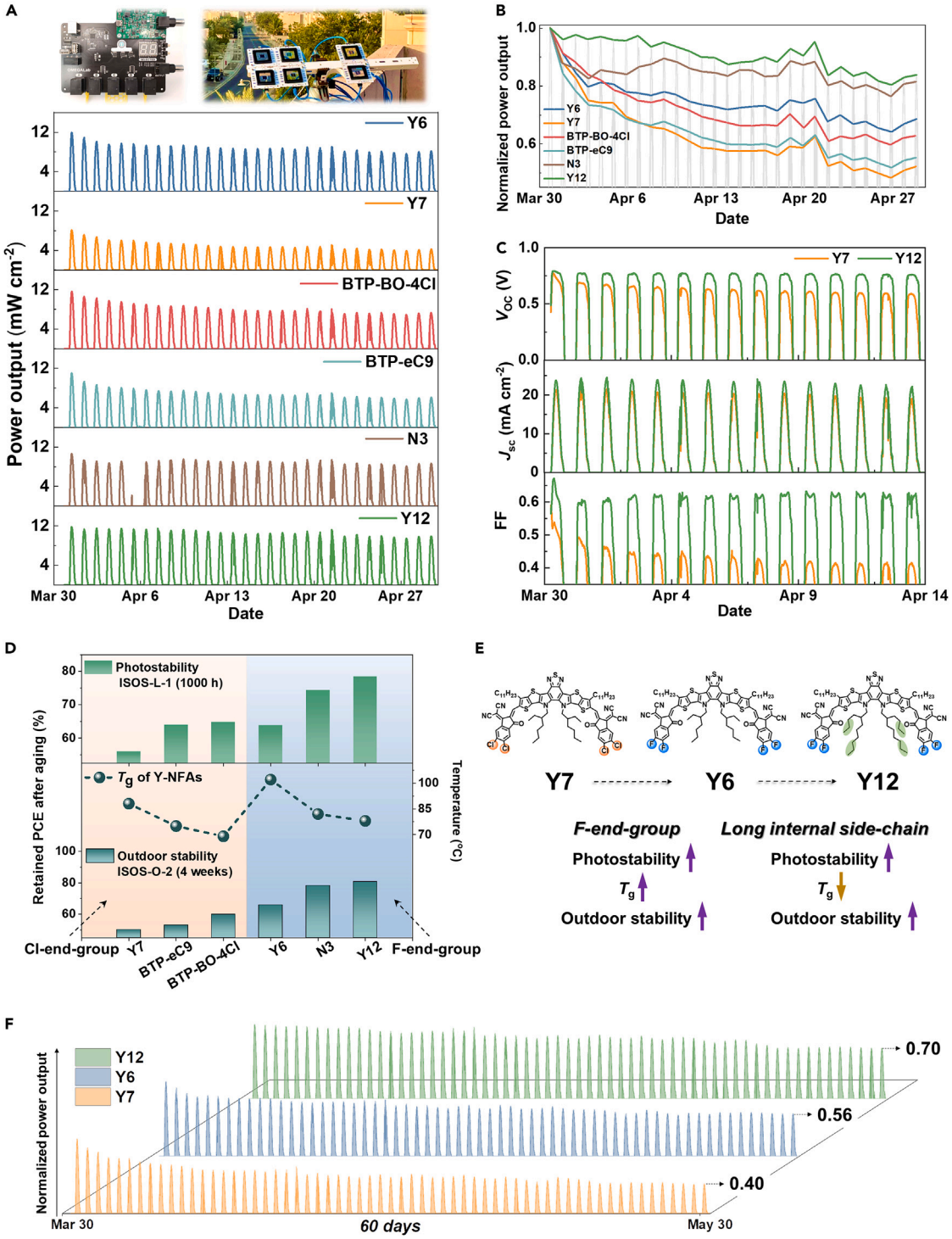

Figure 4. Outdoor performance of Y-NFA cells and structure-stability correlations

(A) Photos of the outdoor setup and outdoor performance of the PM6:Y-NFAs devices (see also Data S1).

(B) Power output changes normalized on the first day.

(C) Parameter change of the Y7- and Y12-based devices during the first 2 weeks.

(D) Relationship between the photostability, T_g, and outdoor stability (KAUST, Saudi Arabia) of the Y-NFA-based OSCs.

(E) Molecular engineering of end-groups and internal side-chains to improve the outdoor stability of Y-NFA cells.

(F) Outdoor stability of the Y7, Y6, and Y12 cells from 30th March to 30th May in the Saudi climate.

10 min. The devices were maintained under open-circuit conditions during the time gaps. Figure 4A also depicts the power output (maximum power point) of devices at different times during the first 4 weeks. Results for longer times are shown in Figure S27. To compare the outdoor stability of these Y-NFA cells (the weather data—solar irradiance and air temperature from 30th March to 30th May; see Figure S28), we normalized the power output by the highest value on the first day of each device and connected the peaks of each day (Figure 4B). The devices fabricated using Y12 and N3 with long internal side-chains remain the two most stable cells, which is similar to their indoor photostability behavior. Moreover, the devices fabricated using the Y-NFAs with fluorinated end groups (Y6 and Y12) still show higher outdoor stability than the chlorinated ones (Y7 and BTP-BO-4Cl). We observed that the BTP-eC9-based device suffered more power output losses than the BTP-BO-4Cl cell in 1 month. The difference mainly comes from the strong burn-in behavior of the BTP-eC9-based device in the first 2 days. By normalizing the third-day maximum power output value, the BTP-BO-4Cl- and BTP-eC9-based devices still have similar degradation rates (Figure S29), indicating that the length of the outer side-chain (–$C_{11}H_{23}$ and –C_9H_{19}) has a negligible effect on their outdoor stability.

We further compared the parameter changes of Y12-based devices (the most stable one) and Y7-based devices (the most unstable one) in the first 2 weeks under outdoor conditions (Figure 4C). The maximum V_{OC} obtained at the highest light irradiance, usually at noon, remains stable for the Y12-based device but decreases gradually for the Y7-based device. Their J_{SC} degradation behaviors are similar and can be further seen in the normalized J_{SC}-date graph (Figure S30). For Y7-based devices, the maximum FF (per day) rapidly dropped from 59.1% to 41.6% after 2 weeks, which could be attributed to the increased recombination losses caused by illumination as exhibited in the photodegradation devices. As a result, the Y12-based device retains 85.3% of its initial power output (per day) after 4 weeks of working under outdoor conditions, which is 1.8 times the retained power output from the Y7-based device (Figure S31).

The temperature of solar cells can reach 65°C–75°C under hot Saudi climates,[76,77] and thermal stress is another factor that degrades OSC devices under outdoor conditions. To correlate further molecular structure with outdoor stability of Y-NFAs, following the Ade-O'Connor-Ghasemi stability framework,[28,29] we plotted glass transition temperature (T_g) of the Y-NFAs together with their photostability and outdoor stability behaviors in Figure 4D (T_g database in Figure S32 and Table S7). It is shown that thermal stability of Y-NFAs is connected to T_g.[29,38] Interestingly, we observe that there is an inverse correlation between thermal stability and outdoor stability when changing the internal side-chain of Y-NFAs. This is due to the fact that long alkyl side-chains can decrease the T_g of Y-NFAs: Y6 > N3 > Y12 and Y7 > BTP-eC9 > BTP-BO-4Cl. In contrast, the steric effect induced by long internal side-chains can suppress the photodegradation pathway of Y-NFAs and thereby improve the photostability of Y-NFA-based solar cells. These results demonstrate that the outdoor stability of Y-NFA-based OSCs with thermal stress under hot Saudi climate is still strongly related to their photostability behaviors under the illumination (temperature ~300 K). Moreover, F-end-groups can improve both the thermal stability and photostability of Y-NFAs. Although BTP-BO-4Cl shows similar degradation behaviors to those of Y6 during the photostability measurements (ISOS-L-1), the Y6-based devices still exhibit better stability than the BTP-BO-4Cl cell under outdoor conditions, which is due to the improved T_g by the F-end- groups in Y6.[29] We then conducted the thermal stability measurements of the devices at 65°C

and 85°C to further clarify the role of heat-induced degradation on the outdoor stability of these Y-NFA-based cells. It is worth mentioning that heat stress not only induces morphology-related degradation but also has a thermal activation effect on the photo-induced chemical degradation of organic materials,[78] both of which can affect the outdoor stability of OSCs. As shown in Figure S33 (Note S7), Y6-based devices are more thermally stable than Y7- and BTP-BO-4Cl-based devices, which can lead to improved outdoor stability. Therefore, the use of a high T_g Y-NFA with low diffusion properties and stable morphology when blended with polymer donors can still benefit the outdoor stability of OSCs. Overall, as shown in Figures 4E and 4F, rational molecular engineering of end-groups and internal side-chains can efficiently improve the outdoor stability of Y-NFA cells. The devices fabricated using Y-NFAs (such as Y12) with fluorinated end-groups and long internal alkyl side-chains exhibit good outdoor stability under real-world operating conditions, showing their potential for outdoor applications.

The lessons and outcomes from the photo- and outdoor stability are as follows. For photostability behaviors of the PM6:Y-NFA-based devices, light-induced chemical structural change is the main reason for the performance loss. Stabilizing the vinyl groups in Y-NFAs is an effective strategy for improving the photostability, such as through the induced steric effect of long internal alkyl side-chains, fluorinated end-group-induced structural confinement in the solid state, and the use of ring-locked end-groups with specific molecular design.[79] Successful encapsulation can effectively prevent oxygen and moisture from degrading PV devices.[27] Under outdoor conditions, solar irradiation and heat are the two main environmental stresses for OSC devices. As observed experimentally, utilizing a strategy for improving both thermal and photostability (introducing fluorinated end-groups) will result in an effective enhancement of outdoor stability for the devices. Our study paves the way for further research on the impact of solar irradiation and heat stress on the outdoor stability of OSCs, which is crucial for scaling up and commercial applications.

Conclusions

We show that the photodegradation of Y-NFA-based OSCs is mainly driven by light-induced trap formation, whereas the change in bimolecular or geminate recombination is limited. The long internal side-chain in Y-NFAs induces high energy barriers for *cis-trans* photoisomerization at the molecular level, and F-end-groups can enhance the structural confinement effect in films. Consequently, devices fabricated using Y12 with fluorinated end-groups and long internal side-chains are more photostable than the other Y-NFA cells. We evaluated the outdoor performance of the encapsulated Y-NFA solar cells by real-time measurement under the Saudi climate via our open-source, affordable μSMU equipment. We demonstrate that the outdoor stability of Y-NFA cells is mainly affected by solar radiation-induced degradation in the hot Saudi climate and still correlates strongly with their photostability behaviors at 300 K. In comparison with Cl-end-groups, F-end-groups can simultaneously enhance photostability and T_g, and thereby stabilize the outdoor performance of Y-NFA solar cells. Although the long internal side-chain decreases the T_g of Y-NFAs, the induced steric effect enhances photostability and still leads to improved outdoor stability of Y-NFA solar cells. The structure-outdoor-stability correlations of Y-NFA cells in this work emphasize the importance of exploring Y-NFAs with stable power output in real-world climates and demonstrate the commercial potential of Y-NFA-based OSCs, thus accelerating the translation of OSC technology.

EXPERIMENTAL PROCEDURES

Resource availability

Lead contact

Further information and requests for resources should be directed to and will be fulfilled by the lead contact, Derya Baran (derya.baran@kaust.edu.sa).

Materials availability

This study did not generate new, unique reagents.

Data and code availability

The outdoor-stability database for the Y-NFA-based devices is available in the supplemental information (Data S1). The data that support the findings of this study are available from the corresponding authors upon reasonable request.

SUPPLEMENTAL INFORMATION

Supplemental information can be found online at https://doi.org/10.1016/j.joule.2023.07.003.

ACKNOWLEDGMENTS

This publication is based upon work supported by the King Abdullah University of Science and Technology (KAUST) Office of Sponsored Research (OSR) under award no. OSR-CARF/CCF-3079 and award no. OSR-CRG2018-3746. We acknowledge the use of the KAUST Solar Center and the support from its staff. J.H. thanks the Alexander von Humboldt Foundation for a Postdoctoral Fellowship. D.B. acknowledges her daughter Ada for being an inspiration for the work on A-D-A structures.

AUTHOR CONTRIBUTIONS

D.B. conceived the idea and directed the project. H.X. and J.H. designed the experiments, fabricated all the solar cell samples, conducted the DFT calculation, and performed the measurements and the data analysis. Y.L. and D.R.V. conducted the Raman spectroscopic measurements. S.C., S.A., and J.G. performed the TDCF measurements and analysis of the results supervised by F.L., L.H.H., J.B., and J.T. built the outdoor setup and conducted outdoor-stability measurements. M.B. and S.D.W. conducted the encapsulation of outdoor solar cells. S.H.K.P., N.R., and J.M. conducted the GIWAXS measurements. C.H., T.B.M., and B.E. helped with the analysis of DFT calculations. A.S. assisted with the data analysis. The manuscript was written by H.X. and J.H. and edited by all co-authors.

DECLARATION OF INTERESTS

The authors declare no competing interests.

Received: January 17, 2023
Revised: April 20, 2023
Accepted: July 3, 2023
Published: July 24, 2023

REFERENCES

1. Bihar, E., Corzo, D., Hidalgo, T.C., Rosas-Villalva, D., Salama, K.N., Inal, S., and Baran, D. (2020). Fully inkjet-printed, ultrathin and conformable organic photovoltaics as power source based on cross-linked PEDOT:PSS electrodes. Adv. Mater. Technol. *5*, 2000226. https://doi.org/10.1002/admt.202000226.

2. Sun, Y., Chang, M., Meng, L., Wan, X., Gao, H., Zhang, Y., Zhao, K., Sun, Z., Li, C., Liu, S., et al. (2019). Flexible organic photovoltaics based on water-processed silver nanowire electrodes. Nat. Electron. *2*, 513–520. https://doi.org/10.1038/s41928-019-0315-1.

3. Fukuda, K., Yu, K., and Someya, T. (2020). The future of flexible organic solar cells. Adv.

Energy Mater. *10*, 2000765. https://doi.org/10.1002/aenm.202000765.

4. Li, Y., Huang, X., Sheriff, H.K.M., and Forrest, S.R. (2022). Semitransparent organic photovoltaics for building-integrated photovoltaic applications. Nat. Rev. Mater. *8*, 186–201. https://doi.org/10.1038/s41578-022-00514-0.

5. Wu, Q., Yu, Y., Xia, X.X., Gao, Y.H., Wang, T., Sun, R., Guo, J., Wang, S.S., Xie, G.H., Lu, X.H., et al. (2022). High-performance organic photovoltaic modules using eco-friendly solvents for various indoor application scenarios. Joule *6*, 2138–2151. https://doi.org/10.1016/j.joule.2022.07.001.

6. Burgués-Ceballos, I., Lucera, L., Tiwana, P., Ocytko, K., Tan, L.W., Kowalski, S., Snow, J., Pron, A., Bürckstümmer, H., Blouin, N., and Morse, G. (2021). Transparent organic photovoltaics: a strategic niche to advance commercialization. Joule *5*, 2261–2272. https://doi.org/10.1016/j.joule.2021.07.004.

7. Corzo, D., Rosas-Villalva, D., C, A., Tostado-Blázquez, G., Alexandre, E.B., Hernandez, L.H., Han, J., Xu, H., Babics, M., De Wolf, S., et al. (2022). High-performing organic electronics using terpene green solvents from renewable feedstocks. Nat. Energy *8*, 62–73. https://doi.org/10.1038/s41560-022-01167-7.

8. Riede, M., Spoltore, D., and Leo, K. (2021). Organic solar cells - the path to commercial success. Adv. Energy Mater. *11*, 2002653. https://doi.org/10.1002/aenm.202002653.

9. Chang, S.-Y., Cheng, P., Li, G., and Yang, Y. (2018). Transparent polymer photovoltaics for solar energy harvesting and beyond. Joule *2*, 1039–1054. https://doi.org/10.1016/j.joule.2018.04.005.

10. Wang, D., Liu, H., Li, Y., Zhou, G., Zhan, L., Zhu, H., Lu, X., Chen, H., and Li, C.-Z. (2021). High-performance and eco-friendly semitransparent organic solar cells for greenhouse applications. Joule *5*, 945–957. https://doi.org/10.1016/j.joule.2021.02.010.

11. Zhang, G., Lin, F.R., Qi, F., Heumüller, T., Distler, A., Egelhaaf, H.J., Li, N., Chow, P.C.Y., Brabec, C.J., Jen, A.K., and Yip, H.L. (2022). Renewed prospects for organic photovoltaics. Chem. Rev. *122*, 14180–14274. https://doi.org/10.1021/acs.chemrev.1c00955.

12. Ravishankar, E., Booth, R.E., Saravitz, C., Sederoff, H., Ade, H.W., and O'Connor, B.T. (2020). Achieving net zero energy greenhouses by integrating semitransparent organic solar cells. Joule *4*, 490–506. https://doi.org/10.1016/j.joule.2019.12.018.

13. Lin, Y., Wang, J., Zhang, Z.-G., Bai, H., Li, Y., Zhu, D., and Zhan, X. (2015). An electron acceptor challenging fullerenes for efficient polymer solar cells. Adv. Mater. *27*, 1170–1174. https://doi.org/10.1002/adma.201404317.

14. Holliday, S., Ashraf, R.S., Wadsworth, A., Baran, D., Yousaf, S.A., Nielsen, C.B., Tan, C.-H., Dimitrov, S.D., Shang, Z., Gasparini, N., et al. (2016). High-efficiency and air-stable P3HT-based polymer solar cells with a new non-fullerene acceptor. Nat. Commun. *7*, 11585. https://doi.org/10.1038/ncomms11585.

15. Meng, D., Zheng, R., Zhao, Y., Zhang, E., Dou, L., and Yang, Y. (2022). Near-infrared materials: the turning point of organic photovoltaics. Adv. Mater. *34*, e2107330. https://doi.org/10.1002/adma.202107330.

16. Yan, C., Barlow, S., Wang, Z., Yan, H., Jen, A.K.-Y., Marder, S.R., and Zhan, X. (2018). Non-fullerene acceptors for organic solar cells. Nat. Rev. Mater. *3*, 18003. https://doi.org/10.1038/natrevmats.2018.3.

17. Yuan, J., Zhang, Y., Zhou, L., Zhang, G., Yip, H.-L., Lau, T.-K., Lu, X., Zhu, C., Peng, H., Johnson, P.A., et al. (2019). Single-junction organic solar cell with over 15% efficiency using fused-ring acceptor with electron-deficient core. Joule *3*, 1140–1151. https://doi.org/10.1016/j.joule.2019.01.004.

18. Li, S., Li, C.-Z., Shi, M., and Chen, H. (2020). New phase for organic solar cell research: Emergence of Y-series electron acceptors and their perspectives. ACS Energy Lett. *5*, 1554–1567. https://doi.org/10.1021/acsenergylett.0c00537.

19. Lin, F., Jiang, K., Kaminsky, W., Zhu, Z., and Jen, A.K.Y. (2020). A non-fullerene acceptor with enhanced intermolecular π-core interaction for high-performance organic solar cells. J. Am. Chem. Soc. *142*, 15246–15251. https://doi.org/10.1021/jacs.0c07083.

20. Li, C., Zhou, J., Song, J., Xu, J., Zhang, H., Zhang, X., Guo, J., Zhu, L., Wei, D., Han, G., et al. (2021). Non-fullerene acceptors with branched side chains and improved molecular packing to exceed 18% efficiency in organic solar cells. Nat. Energy *6*, 605–613. https://doi.org/10.1038/s41560-021-00820-x.

21. Zhu, L., Zhang, M., Xu, J., Li, C., Yan, J., Zhou, G., Zhong, W., Hao, T., Song, J., Xue, X., et al. (2022). Single-junction organic solar cells with over 19% efficiency enabled by a refined double-fibril network morphology. Nat. Mater. *21*, 656–663. https://doi.org/10.1038/s41563-022-01244-y.

22. Bi, P.Q., Zhang, S.Q., Chen, Z.H., Xu, Y., Cui, Y., Zhang, T., Ren, J.Z., Qin, J.Z., Hong, L., Hao, X.T., and Hou, J.H. (2021). Reduced non-radiative charge recombination enables organic photovoltaic cell approaching 19% efficiency. Joule *5*, 2408–2419. https://doi.org/10.1016/j.joule.2021.06.020.

23. Cheng, P., and Zhan, X. (2016). Stability of organic solar cells: challenges and strategies. Chem. Soc. Rev. *45*, 2544–2582. https://doi.org/10.1039/C5CS00593K.

24. Reese, M.O., Gevorgyan, S.A., Jørgensen, M., Bundgaard, E., Kurtz, S.R., Ginley, D.S., Olson, D.C., Lloyd, M.T., Morvillo, P., Katz, E.A., et al. (2011). Consensus stability testing protocols for organic photovoltaic materials and devices. Sol. Energy Mater. Sol. Cells *95*, 1253–1267. https://doi.org/10.1016/j.solmat.2011.01.036.

25. Duan, L., and Uddin, A. (2020). Progress in stability of organic solar cells. Adv. Sci. (Weinh) *7*, 1903259. https://doi.org/10.1002/advs.201903259.

26. Du, X., Heumueller, T., Gruber, W., Classen, A., Unruh, T., Li, N., and Brabec, C.J. (2019). Efficient polymer solar cells based on non-fullerene acceptors with potential device lifetime approaching 10 years. Joule *3*, 215–226. https://doi.org/10.1016/j.joule.2018.09.001.

27. Azmi, R., Ugur, E., Seitkhan, A., Aljamaan, F., Subbiah, A.S., Liu, J., Harrison, G.T., Nugraha, M.I., Eswaran, M.K., Babics, M., et al. (2022). Damp heat-stable perovskite solar cells with tailored-dimensionality 2D/3D heterojunctions. Science *376*, 73–77. https://doi.org/10.1126/science.abm5784.

28. Ghasemi, M., Balar, N., Peng, Z., Hu, H., Qin, Y., Kim, T., Rech, J.J., Bidwell, M., Mask, W., McCulloch, I., et al. (2021). A molecular interaction-diffusion framework for predicting organic solar cell stability. Nat. Mater. *20*, 525–532. https://doi.org/10.1038/s41563-020-00872-6.

29. Qin, Y.P., Balar, N., Peng, Z.X., Gadisa, A., Angunawela, I., Bagui, A., Kashani, S., Hou, J.H., and Ade, H. (2021). The performance-stability conundrum of BTP-based organic solar cells. Joule *5*, 2129–2147. https://doi.org/10.1016/j.joule.2021.06.006.

30. Yu, L.Y., Qian, D.P., Marina, S., Nugroho, F.A.A., Sharma, A., Hultmark, S., Hofmann, A.I., Kroon, R., Benduhn, J., Smilgies, D.M., et al. (2019). Diffusion-limited crystallization: a rationale for the thermal stability of non-fullerene solar cells. ACS Appl. Mater. Interfaces *11*, 21766–21774. https://doi.org/10.1021/acsami.9b04554.

31. Zou, Y.P., and Ye, L. (2021). Stabilizing the microstructure for Y6-series nonfullerene solar cells. Chem *7*, 2853–2854. https://doi.org/10.1016/j.chempr.2021.10.009.

32. Che, Y., Niazi, M.R., Izquierdo, R., and Perepichka, D.F. (2021). Mechanism of the photodegradation of A-D-A acceptors for organic photovoltaics*. Angew. Chem. Int. Ed. Engl. *60*, 24833–24837. https://doi.org/10.1002/anie.202109357.

33. Clarke, A.J., Luke, J., Meitzner, R., Wu, J., Wang, Y., Lee, H.K.H., Speller, E.M., Bristow, H., Cha, H., Newman, M.J., et al. (2021). Non-fullerene acceptor photostability and its impact on organic solar cell lifetime. Physiol. Sci. *2*, 100498. https://doi.org/10.1016/j.xcrp.2021.100498.

34. Liu, Z.X., Yu, Z.P., Shen, Z., He, C., Lau, T.K., Chen, Z., Zhu, H., Lu, X., Xie, Z., Chen, H., and Li, C.Z. (2021). Molecular insights of exceptionally photostable electron acceptors for organic photovoltaics. Nat. Commun. *12*, 3049. https://doi.org/10.1038/s41467-021-23389-1.

35. Luke, J., Yang, E.J., Chin, Y.C., Che, Y.X., Winkler, L., Whatling, D., Labanti, C., Park, S.Y., and Kim, J.S. (2022). Strong intermolecular interactions induced by high quadrupole moments enable excellent photostability of non-fullerene acceptors for organic photovoltaics. Adv. Energy Mater. *12*, 2201267. https://doi.org/10.1002/aenm.202201267.

36. Luke, J., Speller, E.M., Wadsworth, A., Wyatt, M.F., Dimitrov, S., Lee, H.K.H., Li, Z., Tsoi, W.C., McCulloch, I., Bagnis, D., et al. (2019). Twist and degrade-impact of molecular structure on the photostability of nonfullerene acceptors and their photovoltaic blends. Adv. Energy Mater. *9*, 1803755. https://doi.org/10.1002/aenm.201803755.

37. Zhou, B.J., Wang, L., Liu, Y., Guo, C.H., Li, D.H., Cai, J.L., Fu, Y.W., Chen, C., Liu, D., Zhou, Y.H., et al. (2022). On the stability of non-fullerene acceptors and their corresponding organic solar cells: influence of side chains. Adv. Funct. Mater. *32*, 2206042. https://doi.org/10.1002/adfm.202206042.

38. Fan, B., Gao, W., Wu, X., Xia, X., Wu, Y., Lin, F.R., Fan, Q., Lu, X., Li, W.J., Ma, W., and Jen, A.K.Y. (2022). Importance of structural hinderance in performance–stability equilibrium of organic photovoltaics. Nat. Commun. *13*, 5946. https://doi.org/10.1038/s41467-022-33754-3.

39. Khenkin, M.V., Katz, E.A., Abate, A., Bardizza, G., Berry, J.J., Brabec, C., Brunetti, F., Bulović, V., Burlingame, Q., Di Carlo, A., et al. (2020). Consensus statement for stability assessment and reporting for perovskite photovoltaics based on ISOS procedures. Nat. Energy *5*, 35–49. https://doi.org/10.1038/s41560-019-0529-5.

40. Zhang, Y.W., Samuel, I.D.W., Wang, T., and Lidzey, D.G. (2018). Current status of outdoor lifetime testing of organic photovoltaics. Adv. Sci. *5*, 1800434. https://doi.org/10.1002/advs.201800434.

41. Greenbank, W., Djeddaoui, N., Destouesse, E., Lamminaho, J., Prete, M., Boukezzi, L., Ebel, T., Bessissa, L., Rubahn, H.-G., Turkovic, V., and Madsen, M. (2020). Degradation behavior of scalable nonfullerene organic solar cells assessed by outdoor and indoor ISOS stability protocols. Energy Technol. *8*, 2000295. https://doi.org/10.1002/ente.202000295.

42. Josey, D.S., Nyikos, S.R., Garner, R.K., Dovijarski, A., Castrucci, J.S., Wang, J.M., Evans, G.J., and Bender, T.P. (2017). Outdoor performance and stability of boron subphthalocyanines applied as electron acceptors in fullerene-free organic photovoltaics. ACS Energy Lett. *2*, 726–732. https://doi.org/10.1021/acsenergylett.6b00716.

43. Rodríguez-Martínez, X., Riera-Galindo, S., Aguirre, L.E., Campoy-Quiles, M., Arwin, H., and Inganäs, O. (2023). Laminated organic photovoltaic modules for agrivoltaics and beyond: An outdoor stability study of all-polymer and polymer:small molecule blends. Adv. Funct. Materials *33*, 2213220. https://doi.org/10.1002/adfm.202213220.

44. Cui, Y., Yao, H., Zhang, J., Zhang, T., Wang, Y., Hong, L., Xian, K., Xu, B., Zhang, S., Peng, J., et al. (2019). Over 16% efficiency organic photovoltaic cells enabled by a chlorinated acceptor with increased open-circuit voltages. Nat. Commun. *10*, 2515. https://doi.org/10.1038/s41467-019-10351-5.

45. Cui, Y., Yao, H., Hong, L., Zhang, T., Tang, Y., Lin, B., Xian, K., Gao, B., An, C., Bi, P., et al. (2020). Organic photovoltaic cell with 17% efficiency and superior processability. Natl. Sci. Rev. *7*, 1239–1246. https://doi.org/10.1093/nsr/nwz200.

46. Cui, Y., Yao, H., Zhang, J., Xian, K., Zhang, T., Hong, L., Wang, Y., Xu, Y., Ma, K., An, C., et al. (2020). Single-junction organic photovoltaic cells with approaching 18% efficiency. Adv. Mater. *32*, e1908205. https://doi.org/10.1002/adma.201908205.

47. Jiang, K., Wei, Q., Lai, J.Y.L., Peng, Z., Kim, H.K., Yuan, J., Ye, L., Ade, H., Zou, Y., and Yan, H. (2019). Alkyl chain tuning of small molecule acceptors for efficient organic solar cells. Joule *3*, 3020–3033. https://doi.org/10.1016/j.joule.2019.09.010.

48. Hong, L., Yao, H., Wu, Z., Cui, Y., Zhang, T., Xu, Y., Yu, R., Liao, Q., Gao, B., Xian, K., et al. (2019). Eco-compatible solvent-processed organic photovoltaic cells with over 16% efficiency. Adv. Mater. *31*, e1903441. https://doi.org/10.1002/adma.201903441.

49. Wang, Y., Luke, J., Privitera, A., Rolland, N., Labanti, C., Londi, G., Lemaur, V., Toolan, D.T.W., Sneyd, A.J., Jeong, S., et al. (2023). The critical role of the donor polymer in the stability of high-performance non-fullerene acceptor organic solar cells. Joule *7*, 810–829. https://doi.org/10.1016/j.joule.2023.03.002.

50. Martynov, I.V., Inasaridze, L.N., and Troshin, P.A. (2022). Resist or oxidize: identifying molecular structure-photostability relationships for conjugated polymers used in organic solar cells. ChemSusChem *15*, e202101336. https://doi.org/10.1002/cssc.202101336.

51. Brinkmann, K.O., Becker, T., Zimmermann, F., Kreusel, C., Gahlmann, T., Theisen, M., Haeger, T., Olthof, S., Tückmantel, C., Günster, M., et al. (2022). Perovskite-organic tandem solar cells with indium oxide interconnect. Nature *604*, 280–286. https://doi.org/10.1038/s41586-022-04455-0.

52. Zhao, Y., Wu, Z., Liu, X., Zhong, Z., Zhu, R., and Yu, J. (2021). Revealing the photo-degradation mechanism of PM6:Y6 based high-efficiency organic solar cells. J. Mater. Chem. C *9*, 13972–13980. https://doi.org/10.1039/D1TC03655F.

53. Liu, T., Burlingame, Q.C., Ivancevic, M.R., Liu, X., Hu, J., Rand, B.P., and Loo, Y.L. (2023). Photochemical decomposition of Y-series non-fullerene acceptors is responsible for degradation of high-efficiency organic solar cells. Adv. Energy Mater. *13*, 2300046. https://doi.org/10.1002/aenm.202300046.

54. Shi, M., Wang, T., Wu, Y., Sun, R., Wang, W., Guo, J., Wu, Q., Yang, W., and Min, J. (2021). The intrinsic role of molecular mass and polydispersity index in high-performance non-fullerene polymer solar cells. Adv. Energy Mater. *11*, 2002709. https://doi.org/10.1002/aenm.202002709.

55. Fan, B., Gao, W., Zhang, R., Kaminsky, W., Lin, F.R., Xia, X., Fan, Q., Li, Y., An, Y., Wu, Y., et al. (2023). Correlation of local isomerization induced lateral and terminal torsions with performance and stability of organic photovoltaics. J. Am. Chem. Soc. *145*, 5909–5919. https://doi.org/10.1021/jacs.2c13247.

56. Juška, G., Arlauskas, K., Viliūnas, M., Genevičius, K., Österbacka, R., and Stubb, H. (2000). Charge transport in π-conjugated polymers from extraction current transients. Phys. Rev. B *62*, R16235–R16238. https://doi.org/10.1103/PhysRevB.62.R16235.

57. Perdigón-Toro, L., Zhang, H.T., Markina, A.S., Yuan, J., Hosseini, S.M., Wolff, C.M., Zuo, G.Z., Stolterfoht, M., Zou, Y.P., Gao, F., et al. (2020). Barrierless free charge generation in the high-performance PM6:Y6 bulk heterojunction non-fullerene solar cell. Adv. Mater. *32*, e1906763. https://doi.org/10.1002/adma.201906763.

58. Kniepert, J., Lange, I., van der Kaap, N.J., Koster, L.J.A., and Neher, D. (2014). A conclusive view on charge generation, recombination, and extraction in as-prepared and annealed P3HT:PCBM blends: combined experimental and simulation work. Adv. Energy Mater. *4*, 1301401. https://doi.org/10.1002/aenm.201301401.

59. Wu, J.Y., Lee, J., Chin, Y.C., Yao, H.F., Cha, H., Luke, J., Hou, J.H., Kim, J.S., and Durrant, J.R. (2020). Exceptionally low charge trapping enables highly efficient organic bulk heterojunction solar cells. Energy Environ. Sci. *13*, 2422–2430. https://doi.org/10.1039/D0EE01338B.

60. Xian, K., Zhang, S., Xu, Y., Liu, J., Zhou, K., Peng, Z., Li, M., Zhao, W., Chen, Y., Fei, Z., et al. (2023). Refining acceptor aggregation in nonfullerene organic solar cells to achieve high efficiency and superior thermal stability. Sci. China Chem. *66*, 202–215. https://doi.org/10.1007/s11426-022-1394-y.

61. Lee, D., Jang, Y., Kim, J., Jeong, S.Y., Woo, H.Y., Lee, D., Kim, J., Lee, Y., Lee, C., and Lee, W. (2023). Impact of metal oxide diffusion and materials design on thermal stabilities of non-fullerene polymer solar cells. J. Mater. Chem. A *11*, 3008–3017. https://doi.org/10.1039/D2TA07390K.

62. Yao, J., Qiu, B., Zhang, Z.G., Xue, L., Wang, R., Zhang, C., Chen, S., Zhou, Q., Sun, C., Yang, C., et al. (2020). Cathode engineering with perylene-diimide interlayer enabling over 17% efficiency single-junction organic solar cells. Nat. Commun. *11*, 2726. https://doi.org/10.1038/s41467-020-16509-w.

63. Gillett, A.J., Privitera, A., Dilmurat, R., Karki, A., Qian, D.P., Pershin, A., Londi, G., Myers, W.K., Lee, J., Yuan, J., et al. (2021). The role of charge recombination to triplet excitons in organic solar cells. Nature *597*, 666–671. https://doi.org/10.1038/s41586-021-03840-5.

64. Han, G., and Yi, Y. (2022). Singlet-triplet energy gap as a critical molecular descriptor for predicting organic photovoltaic efficiency. Angew. Chem. Int. Ed. Engl. *61*, e202213953. https://doi.org/10.1002/anie.202213953.

65. Lee, H.K.H., Telford, A.M., Röhr, J.A., Wyatt, M.F., Rice, B., Wu, J., de Castro Maciel, A., Tuladhar, S.M., Speller, E., McGettrick, J., et al. (2018). The role of fullerenes in the environmental stability of polymer:fullerene solar cells. Energy Environ. Sci. *11*, 417–428. https://doi.org/10.1039/C7EE02983G.

66. Kupgan, G., Chen, X.-K., and Brédas, J.-L. (2019). Low energetic disorder in small-molecule non-fullerene electron acceptors. ACS Mater. Lett. *1*, 350–353. https://doi.org/10.1021/acsmaterialslett.9b00248.

67. Haneef, H.F., Zeidell, A.M., and Jurchescu, O.D. (2020). Charge carrier traps in organic semiconductors: a review on the underlying physics and impact on electronic devices. J. Mater. Chem. C *8*, 759–787. https://doi.org/10.1039/C9TC05695E.

68. Grüne, J., Londi, G., Gillett, A.J., Stähly, B., Lulei, S., Kotova, M., Olivier, Y., Dyakonov, V., and Sperlich, A. (2023). Triplet excitons and

associated efficiency-limiting pathways in organic solar cell blends based on (non-) halogenated PBDB-T and Y-series. Adv. Funct. Mater. *33*, 2212640. https://doi.org/10.1002/adfm.202212640.

69. Narsaria, A.K., Rauch, F., Krebs, J., Endres, P., Friedrich, A., Krummenacher, I., Braunschweig, H., Finze, M., Nitsch, J., Bickelhaupt, F.M., and Marder, T.B. (2020). Computationally guided molecular design to minimize the LE/CT gap in D-π-A fluorinated triarylboranes for efficient TADF via D and π-bridge tuning. Adv. Funct. Mater. *30*, 2002064. https://doi.org/10.1002/adfm.202002064.

70. Lin, Y.S., Li, G.D., Mao, S.P., and Chai, J.D. (2013). Long-range corrected hybrid density functionals with improved dispersion corrections. J. Chem. Theor. Comput. *9*, 263–272. https://doi.org/10.1021/ct300715s.

71. Zhao, Q.Q., Qu, J.F., and He, F. (2020). Chlorination: an effective strategy for high-performance organic solar cells. Adv. Sci. (Weinh) *7*, 2000509. https://doi.org/10.1002/advs.202000509.

72. Patrick, C.R., and Prosser, G.S. (1960). A molecular complex of benzene and hexafluorobenzene. Nature *187*, 1021. https://doi.org/10.1038/1871021a0.

73. Friedrich, A., Collings, I.E., Dziubek, K.F., Fanetti, S., Radacki, K., Ruiz-Fuertes, J., Pellicer-Porres, J., Hanfland, M., Sieh, D., Bini, R., et al. (2020). Pressure-induced polymerization of polycyclic arene-perfluoroarene cocrystals: single crystal X-ray diffraction studies, reaction kinetics, and design of columnar hydrofluorocarbons. J. Am. Chem. Soc. *142*, 18907–18923. https://doi.org/10.1021/jacs.0c09021.

74. Markina, A., Lin, K.H., Liu, W.L., Poelking, C., Firdaus, Y., Villalva, D.R., Khan, J.I., Paleti, S.H.K., Harrison, G.T., Gorenflot, J., et al. (2021). Chemical design rules for non-fullerene acceptors in organic solar cells. Adv. Energy Mater. *11*, 2102363. https://doi.org/10.1002/aenm.202102363.

75. Xu, H., Torres Merino, L., Koc, M., Aydin, E., Zhumagali, S., Haque, M.A., Yazmaciyan, A., Sharma, A., Rosas Villalva, D., Huerta Hernandez, L., et al. (2022). Metal-free interconnecting layer for monolithic perovskite/organic tandem solar cells with enhanced outdoor stability. ACS Appl. Energy Mater. *5*, 14035–14044. https://doi.org/10.1021/acsaem.2c01749.

76. Aydin, E., Allen, T.G., De Bastiani, M., Xu, L.J., Ávila, J., Salvador, M., Van Kerschaver, E., and De Wolf, S. (2020). Interplay between temperature and bandgap energies on the outdoor performance of perovskite/silicon tandem solar cells. Nat. Energy *5*, 851–859. https://doi.org/10.1038/s41560-020-00687-4.

77. Babics, M., De Bastiani, M., Balawi, A.H., Ugur, E., Aydin, E., Subbiah, A.S., Liu, J., Xu, L.J., Azmi, R., Allen, T.G., et al. (2022). Unleashing the full power of perovskite/silicon tandem modules with solar trackers. ACS Energy Lett. *7*, 1604–1610. https://doi.org/10.1021/acsenergylett.2c00442.

78. Hintz, H., Egelhaaf, H.-J., Lüer, L., Hauch, J., Peisert, H., and Chassé, T. (2011). Photodegradation of P3HT-a systematic study of environmental factors. Chem. Mater. *23*, 145–154. https://doi.org/10.1021/cm102373k.

79. Liu, H.T., Wang, W., Zhou, Y.H., and Li, Z.A. (2021). A ring-locking strategy to enhance the chemical and photochemical stability of A-D-A-type non-fullerene acceptors. J. Mater. Chem. A *9*, 1080–1088. https://doi.org/10.1039/D0TA09924D.